

Calibration of the Planetary Fourier Spectrometer long wavelength channel

M. Giuranna^{a,*}, V. Formisano^a, D. Biondi^a, A. Ekonomov^b, S. Fonti^c, D. Grassi^a,
H. Hirsch^d, I. Khatuntsev^b, N. Ignatiev^{a,b}, M. Malgoska^e, A. Mattana^a,
A. Maturilli^a, E. Mencarelli^a, F. Nespoli^a, R. Orfei^a, P. Orleanski^e,
G. Piccioni^f, M. Rataj^e, B. Saggin^g, L. Zasova^{a,b}

^a*Istituto di Fisica dello Spazio Interplanetario CNR (IFSI), Via del Fosso del Cavaliere 100, 00133 Roma, Italy*

^b*Space Research Institute of Russian Academy of Sciences (IKI), Profsojuznaja 84/32, 117810 Moscow, Russia*

^c*Università degli Studi di Lecce, Dipartimento di Fisica, Via Arnesano, 73100 Lecce, Italy*

^d*Deutsche Forschungsanstalt für Luft und Raumfahrt (DLR), Institut für Planetenerforschung, Rudower Chaussee 5, 12489 Berlin Adlershof, Germany*

^e*Space Research Center of Polish Academy of Sciences (SRC PAS), Bartycka 18A, 00716 Warsaw, Poland*

^f*Istituto Astrofisica Spaziale CNR (IAS), 00185 Roma, Italy*

^g*Università di Padova, Dipartimento Ingegneria Meccanica (DIUNP), Via Venezia 1, 35131 Padova, Italy*

Received 13 April 2004; received in revised form 7 February 2005; accepted 7 February 2005

Available online 13 June 2005

Abstract

The Planetary Fourier Spectrometer (PFS) experiment on board the Mars Express mission has two channels covering the 1.2–5 μm (SWC) and the 5–50 μm (LWC). The Long Wavelength Channel (LWC) measures the thermal emission spectrum of Mars between 200 and 2000 cm^{-1} with a spectral resolution of 1.4 cm^{-1} , in absence of apodisation. We present here the calibration of this channel and its performance. The instrument calibration has been performed on ground, before launch, in space during Near Earth Verification (NEV) measurements, and at Mars. Special attention has been given to the problem of microvibrations on board the spacecraft.

In order to obtain correct results, the source-instrument-detector interaction is studied very accurately. The instrument variations during a pericentre pass impose a complex procedure for the LW channel calibration, but fortunately the procedure adopted seems to work well. Samples of the calibrated data are given (as single spectrum and as an average over a few spectra) to show the performance of the experiment and its scientific potentialities.

© 2005 Elsevier Ltd. All rights reserved.

1. Introduction

This paper is published in the special issue of “Planetary and Space Science” devoted to the first results of the Mars Express PFS investigation. Explanations of the design and operation of the instrument, together with the description of the optical layout, the detectors and signal handling have been given in Paper I (Formisano et al., 2005) of this issue.

The Mars Express spacecraft was successfully launched on 2 June 2003 and is currently orbiting Mars. The Planetary Fourier Spectrometer is one of the seven instruments (plus a lander, *Beagle 2*) on board the spacecraft, and is designed to record the Martian infrared spectrum between 1.2 and 50 μm by means of two interferometers, working simultaneously in two different spectral regions: the short wavelength channel (SWC) selects the radiation in the range 1.2–5 μm , while the long wavelength channel (LWC) covers the range between 5 and 50 μm (200–2000 cm^{-1}). Both channels have a spectral resolution of 1.4 cm^{-1} (samples every

*Corresponding author.

E-mail address: macro.giuranna@ifsi.rm.cnr.it (M. Giuranna).

1 cm^{-1}). PFS produces “double-sided” interferograms; owing to phase errors all original interferograms have an asymmetric form. Asymmetry of the central part of the interferogram has been corrected by means of the specially developed algorithm based on the method of phase correction (Forman and Howard, 1966). We name the corrected interferogram as “symetrised”. More information on the used algorithm can be found in the appendix of Paper III of this issue (Giuranna et al., 2005).

The purpose of this paper is to present the radiometric and spectral performances of the LWC resulting in the ground calibrations first and in space later and presently at Mars.

The LWC detector is a pyroelectric (LiTaO_3 , a $15 \mu\text{m}$ gold film) working at room temperature T_o and it is sensitive to the temperature difference between the emitting source (T_s) and the detector temperature; the amplitude of the measured signal is then depending on $\Delta T = |T_o - T_s|$. The thermal conditions of the instrument are therefore very important: in the laboratory we were not able to stabilise the detector temperature while in space it is well controlled within a few hundreds of a degree.

It is important to note that the LWC of PFS is similar to the IRIS experiment on Mariner 9 mission (Hanel et al., 1970, 1972). However, the basic design is different (a Michelson IRIS, a double pendulum PFS). Also, the working conditions are very different: IRIS was working at 251 K, while PFS works at 287 K (or above) with a detector well stabilised in temperature. Like IRIS we also have on board a calibration Blackbody of known temperature, and we use Deep Space as another calibration Source.

The thermal conditions of the interferometer are also very important for the calibration of the measurements, as the PFS LW channel performs differential measurements, therefore we are sensitive to the instrument temperatures.

2. Laboratory and space measurements

All the measurements performed on Earth and during the Near Earth Verification phase, and a first analysis of these data are listed and described in the PFS Instrument Calibration Report, vol. I, II and III (Formisano et al., 2002, 2003a, b).

2.1. Calibration sources

The PFS LWC has been calibrated in laboratory mainly by means of two calibration sources:

- The “IFSI” blackbody (MIKRON M345 \times 4 UDC), with a manufacturer certified emissivity of 0.970 ± 0.005

in the ranges 8–15 and 3–5 μm . Thanks to a control panel it is possible to set its temperature with a precision of one hundredth of a degree, up to a maximum of 150 °C. The chosen temperature turns out to be extremely stable during all the acquisition sessions, with oscillations that do not exceed $\pm 0.01 \text{ K}$, although it is necessary to wait approximately 15 min for a thermal stabilisation.

- The “IKI” blackbody, developed in Russia, but available in IFSI with an emissivity of 1.0 ± 0.1 estimated by us, in laboratory measurements in Lecce. No temperature control panel is provided.

Unfortunately, none of the two blackbodies could work in a vacuum chamber and it was not easy to set up measurements with a source at temperature lower than the detector and instrument temperature. However, it is necessary to study the response of the instrument also for sources far below the 25–30 °C of the laboratory, in order not only to cover the expected Martian temperatures, but also to compare the responsivity of the detector when observing sources with brightness temperatures greater or smaller than that of the detector itself. For this purpose we used the IKI Blackbody, with which it has been possible to reach temperatures as low as -100 °C , thanks to a CO_2 ambient cage atmosphere and a Nitrogen-based cooling system.

PFS has a built-in blackbody; its thermal and spectral properties (i.e. temperature uniformity and emissivity) have been extensively studied in laboratory and it is used as a calibration source in space, together with the deep-space observations. For the internal blackbody it is not possible to set up a temperature, which comes therefore to depend mainly on the room temperature.

A detailed list of the measurements performed in laboratory, for both IFSI and IKI blackbodies, is given in Table 1. In addition, 200 acquisitions were taken looking at the internal blackbody while the PFS was in the thermovacuum chamber.

Table 1
Calibration measurements in laboratory

T (°C)	No of acquisitions
<i>IFSI Blackbody</i>	
30	200
40	200
50	400
100	200
148.9	200
<i>IKI Blackbody</i>	
0	200
-30	200
-60	200
-100	200

During the NEV phase, few hundreds of calibration measurements were taken looking at the internal blackbody and pointing the scanner toward deep-space; occasionally, the speed of double-pendulum was changed from its default value (2000 Hz) to investigate the double pendulum speed effect on the spectra in relation to mechanical microvibrations.

2.2. Effects of the external mechanical vibrations

It is well known that in interferometric measurements the sampling step of the interferograms, in terms of optical path difference, must be as constant as possible and therefore so must be the movable mirror speed. As described in Paper I, an external mechanical vibration present on the MEX spacecraft is responsible for a non-uniform motion of the double-pendulum: time intervals between contiguous zero-crossings of a reference laser diode interferogram should be close to 250 μ s for nominal speed (also called “speed 2000 Hz”); autotests performed in space always showed strong modulations around this value.

The PFS LW channel has a band-pass filter, whose actual range is related to the speed of the pendulum and the sampling frequency: for nominal speed, filter’s frequencies are 50–500 Hz for the LWC. The frequencies of the mechanical disturbances are some within the band and some outside it. We actually see the effect of all the frequencies of the mechanical vibrations in the spectra either directly or by aliasing. Deep study of the details shows that, thanks to the special optical and mechanical design of the PFS, the effect of such vibrations is only to

induce a fluctuation in the integration time of the measured signal which, in turn, causes an increase of the instrumental noise in special narrow bands. Fig. 1 shows average and standard deviation (sigma) of a set of measurements acquired during NEV tests looking at deep-space. Sigma has values between 0.06 and 0.08 almost everywhere. Two peaks go up to 0.4 (a factor 5 higher), while a smaller peak is observed going up to 0.1. These peaks are at 1660 and 1880 cm^{-1} ; the small peak is at 400 cm^{-1} (100 Hz): another peak should be present at 2180 cm^{-1} , but it is out of the LW range.

This can be explained as follows: the mechanical vibrations have three fundamental frequencies, $\nu_1 = 10\text{--}20$ Hz, $\nu_2 = 105\text{--}110$ Hz and $\nu_3 = 595\text{--}600$ Hz, modulating each other (satellites); each peak is generated by a well-defined vibration and its position in the spectrum is equivalent in frequency to the one of the mechanical vibration. Referring to Fig. 1, the first two peaks are actually aliasing from 595 Hz (ν_3) and 545 Hz the latter being a satellite of ν_3 . The third peak is generated directly by the 545 Hz satellite. The small peak at 400 cm^{-1} corresponds to ν_2 . The same peaks are present when looking at the internal blackbody or at the calibration lamp with the LW channel.

2.3. The effects of changing the speed of double-pendulum

By changing the speed of the pendulum, therefore changing band-pass frequencies range, we are able to move the vibration disturbances from a portion of the spectrum (in cm^{-1}) to another, leaving the rest clean and uncontaminated. We used four different speeds, namely

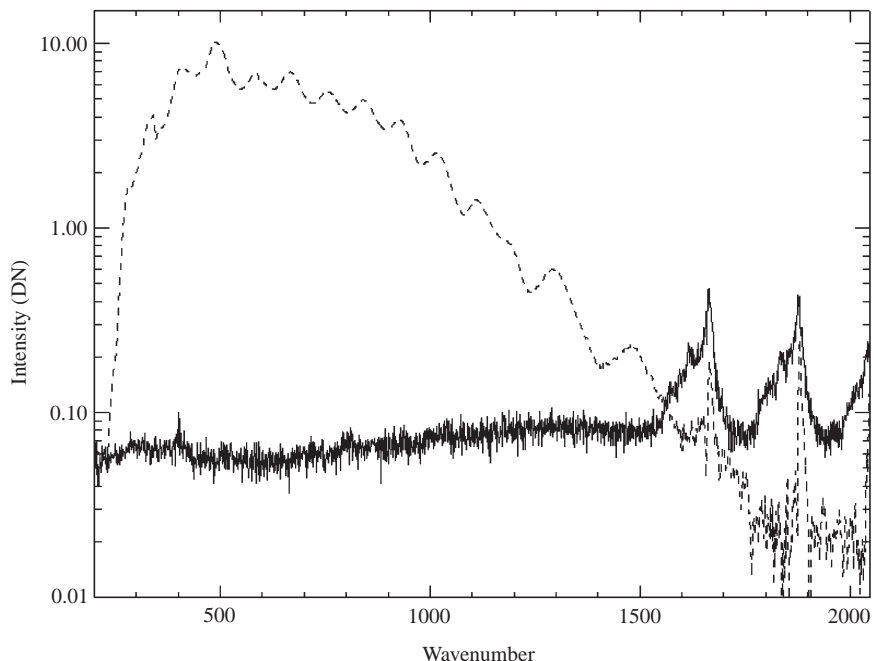


Fig. 1. Deep-space observation. Average spectrum (dashed) and sigma (line) in the LW channel.

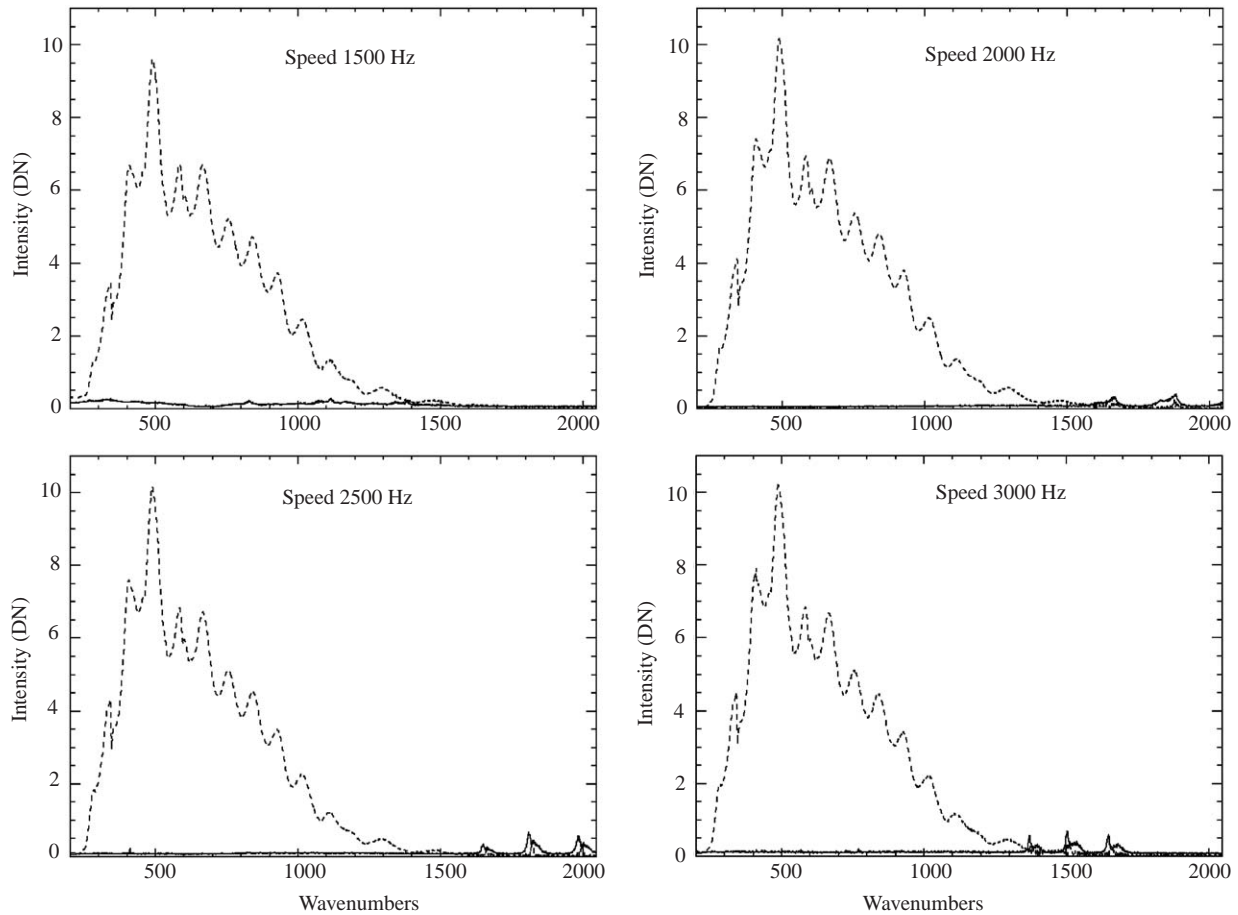


Fig. 2. The effect of the mechanical vibrations for different speeds. Averages and standard deviations are showed. See text for details.

1500, 2000, 2500 and 3000 Hz; the resulting average spectra and standard deviations for the deep-space observations are shown in Fig. 2. We note the apparent absence of major disturbances due to mechanical vibrations when the speed was 1500 Hz, while for higher speeds we see two or three peaks in the standard deviations, which may be reflected in artefacts in the averaged spectra too. The position of these peaks is changing with the speed: they seem to enter from right side and move toward the centre of the spectral range; moreover, the actual intensity of the disturbances is increasing with increasing speed. The vertical linear scale used for this figure allows a direct comparison of the peaks intensity, both in the spectrum and in the noise, with respect to the signal intensity.

These results are understood as a direct consequence of the speed changing: at low speed the vibration frequencies may be out of the frequency range of the channel and the disturbances present in the channel cause only a small jitter of the optical path difference increment.

From Fig. 2 it is evident that the lower the speed of the pendulum, the better the situation of the LW channel,

and one may conclude that speed 1500 Hz should be preferred; but in order to select the best speed for the experiment we also have to consider the SW channel (see the following paper Giuranna et al., 2005). Here we note that from 1500 to 2000 cm^{-1} the wave number range is of lower scientific interest, at least if compared to 400–800 cm^{-1} or 800–1300 cm^{-1} ranges. Disturbances below 1500 cm^{-1} should be avoided. The range 1600–2000 cm^{-1} is also well covered by the SW channel, as we shall see in the Giuranna et al. SW calibration paper. From these and others considerations, we conclude that speed 2500 Hz is probably the best.

In any case, when on Mars we shall have the possibility to repeat measurements with different speeds, in order to cover the whole LWC spectral range with a good SNR. Outside the spectral range affected by the vibration disturbances, all the faint spectral features are reliable; this can be predicted by looking at Fig. 2, where all the standard deviations show no narrow features outside this range (which depends on the speed of the double-pendulum) and has been confirmed by fitting the Martian observations with synthetic spectra (see Fig. 19 at the end of this paper).

3. Modelling the detector–instrument–source interaction

The amplitude $S(\nu)$ of a PFS LW channel spectrum is proportional to the difference between the incoming radiance of the target $I(\nu)$ and the emission of the instrument $I_o(\nu)$:

$$|S(\nu)| = R(\nu)|I(\nu) - I_o(\nu)|. \quad (3.1)$$

The factor of proportionality $R(\nu)$ is the responsivity of the instrument. The emission of the instrument $I_o(\nu)$ depends essentially on its temperature; the instrumental thermal conditions are therefore very important and should be conveniently described and modelled. If the thermal conditions of the instrument are stable, which means $I_o(\nu)$ remaining constant during different observations, we can obtain the responsivity directly from Eq. (3.1) simply by observing a reference blackbody with two different temperatures and thus eliminating $I_o(\nu)$. Unfortunately, this is not the situation neither in laboratory, nor in space, because the instrument is not one block at the same temperature, but it is made of two parts: the detector and the optical bench. The detector temperature was not stable in the measurements on ground (see Fig. 3), while the interferometer temperature normally is not stable in space (Fig. 4).

In order to achieve the best interaction model we tried different approaches and the results are different when in laboratory or in space.

3.1. Calibrations from laboratory measurements

During all the calibration measurements done in the laboratory, the detector temperature and the interferometer temperature were almost the same, the second being a little higher than the first. Despite this, we found that the best approach to describe the detector–sour-

ce–instrument interaction was to consider the effective instrument temperature, which is somewhere between those of the interferometer and the detector. So we could write

$$I_o(\nu) = B(T_{\text{eff}}, \nu) = \alpha(n)B(T_i, \nu) + [1 - \alpha(n)]B(T_d, \nu), \quad (3.2)$$

where T_i is the interferometer temperature (the mean value of the eight thermometers temperatures), T_d the detector temperature (as read by the housekeeping data) and the parameter α may assume values between zero and one. This method was first suggested by Hanel et al. (1992). If instrument and detector are exactly at the same temperature, clearly α is one. In general, α deviates from unity and may vary also with wave number. With two different measurements and using (3.2) into (3.1) we can, in principle, obtain both $R(\nu)$ and $\alpha(\nu)$ by a simple two-equations algebraic system; but since, T_i and T_d are very similar, the system results to be unstable and it has not been possible to obtain acceptable values for $\alpha(\nu)$ in this way. However, considering α as a free parameter, independent from ν , we have

$$R(\nu) = \frac{S(\nu)}{I(\nu) - \alpha B(T_i, \nu) - (1 - \alpha)B(T_d, \nu)}. \quad (3.3)$$

Using the calibration measurements shown in Table 1, by means of Eq. (3.3) we can obtain a set of responsivities for different sources. Since the responsivity is an intrinsic property of the instrument, it is independent from the target brightness and the curves must be identical: we can set the proper value for α by varying it from 0 to 1 with steps of 0.01 and selecting the value that minimises the differences between the responsivities. In this way, we were able to obtain excellent results: α was 0.97 and the curves differ for no more than $\pm 1\%$.

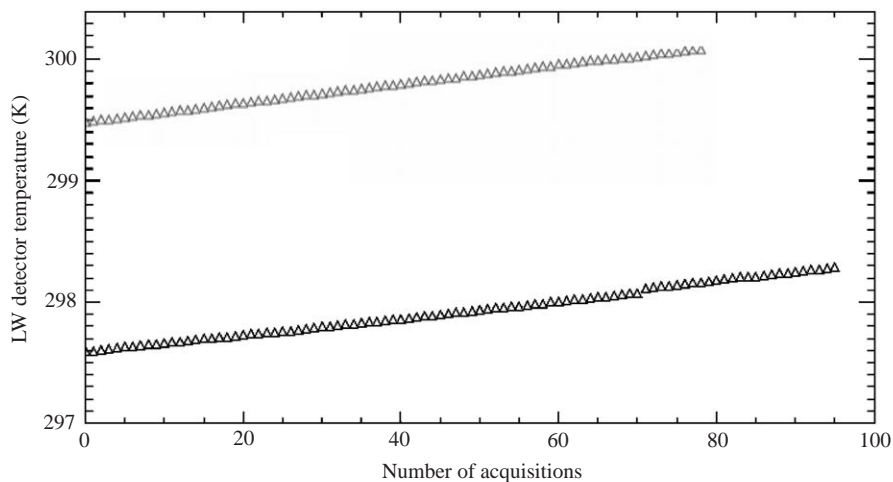


Fig. 3. LWC detector temperature variations during a session of measurements with the IFSI BB at 30 °C (bottom) and 50 °C (top)—laboratory measurements.

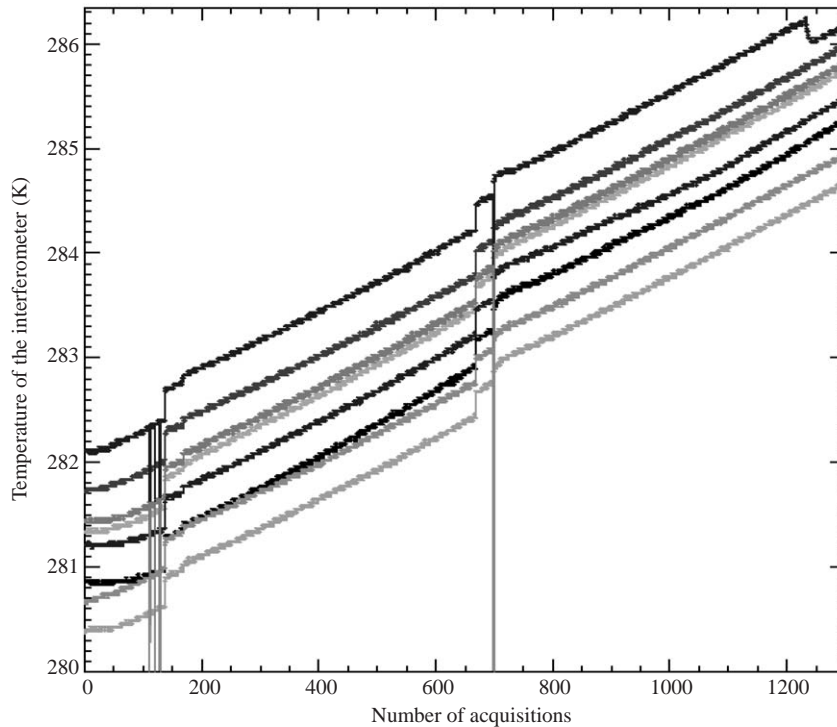


Fig. 4. Temperature of the interferometer monitored by eight thermometers during the NEV activity.

The detailed structure of the responsivity curve is determined primarily by the properties of the beam splitter coatings, the transmission characteristic of the entrance window and the spectral response of the detector. Since the measurements were taken in air, some H₂O and CO₂ features were present, which of course are absent in space.

The averaged responsivities obtained with IFSI and IKI blackbodies are shown in Fig. 5. The curves are different and this is understood as a different behaviour of the detector when observing sources warmer or colder than its own temperature. This is a very important point as it brings us to the conclusion to avoid having the instrument stabilised at a temperature similar to the ones we aim to measure. The responsivity of the interferometer is different above or below the instrument temperature because the interaction with the source is different. We may have two different linear behaviours in the two regimes. The detector is linear, but with different coefficients for cold and hot sources, the responsivity being higher in the first case. This is also confirmed by laboratory measurements.

With the responsivities given above we were able to study the internal Blackbody which was found to have an emissivity of 0.99 as shown in Fig. 6.

3.2. The noise equivalent radiance (NER)

Once we have the responsivity, and therefore the radiance, we can compute the NER, that represents the

radiance that a source must have in order to produce a signal equal to that generated from the instrumental noise; in other words, the minimum detectable signal. For a fixed source and for every measurement, the radiance “as seen” by the PFS can be expressed as follows:

$$b_{i,T}(v) = \frac{S_{i,T}(v)}{R(v)}, \quad (3.4)$$

where $S_{i,T}(v)$ is the i th spectrum of a measurement session with a blackbody at a temperature T and $R(v)$ is the responsivity previously computed by means of Eq. (3.3).

Using all the spectra for the various temperatures, the NER is given by

$$\text{NER}(v) = \sqrt{\frac{\sum_T \sum_i [b_{i,T}(v) - \bar{b}_T(v)]^2}{n}}, \quad (3.5)$$

where \bar{b}_T is the average radiance per temperature and n is the total number of spectra.

An estimate of the PFS NER has been obtained from the measurements listed in Table 1; the results are shown in Fig. 7. The two curves do not show substantial differences, which is an index of a high stability of the instrument.

Although more noisy than those obtained from the IFSI blackbody, the mean values above 1500 cm⁻¹ of both responsivity and NER obtained with the IKI blackbody are trustable and later confirmed by the NEV

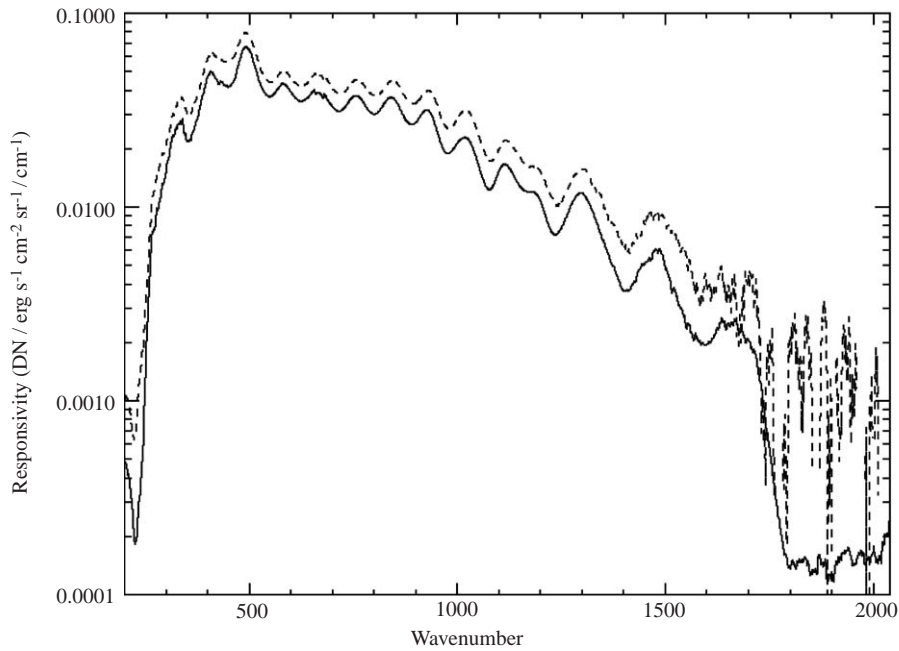


Fig. 5. Average responsivity of PFS LW channel obtained with IFSI (line) and IKI (dashed) blackbodies. In the first case, the source was warmer than the detector temperature while in the second case it was colder.

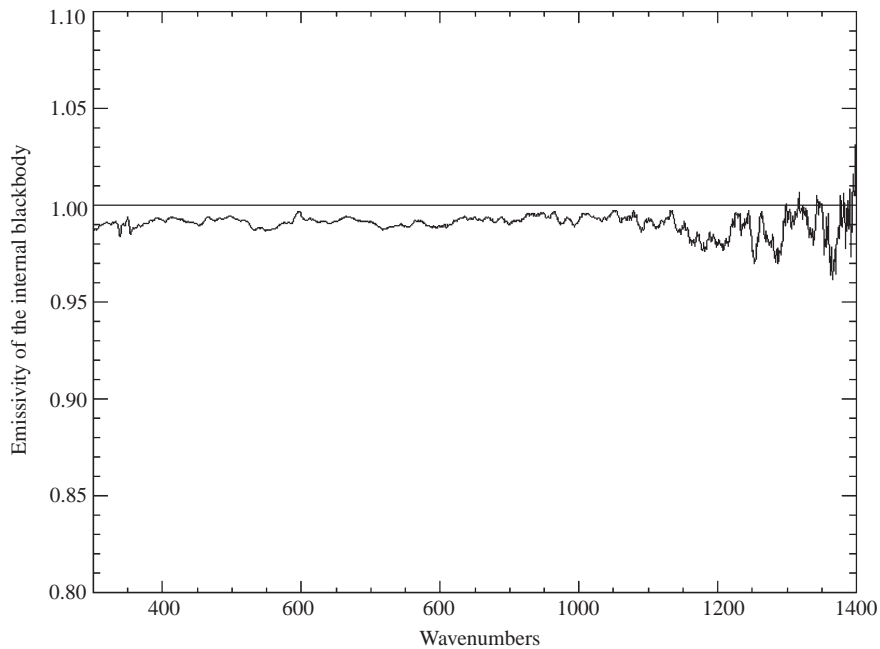


Fig. 6. Emissivity of the internal blackbody. Above 1400 cm^{-1} the measurements are noisy: the detector and the internal BB were very close in temperature.

calibration results. The curves show the water lines and the CO_2 features. We repeated the NER computation using the measurements done in the thermovacuum chamber looking at the internal blackbody; the curve is very smooth, as can be seen in Fig. 8, and was adopted as the official PFS NER in laboratory.

3.3. NEV results

The temperature of the LW channel detector should, in theory, be controlled and stable with an accuracy of 0.01 K. While on Earth we were not able to control it, since the room temperature was higher than the

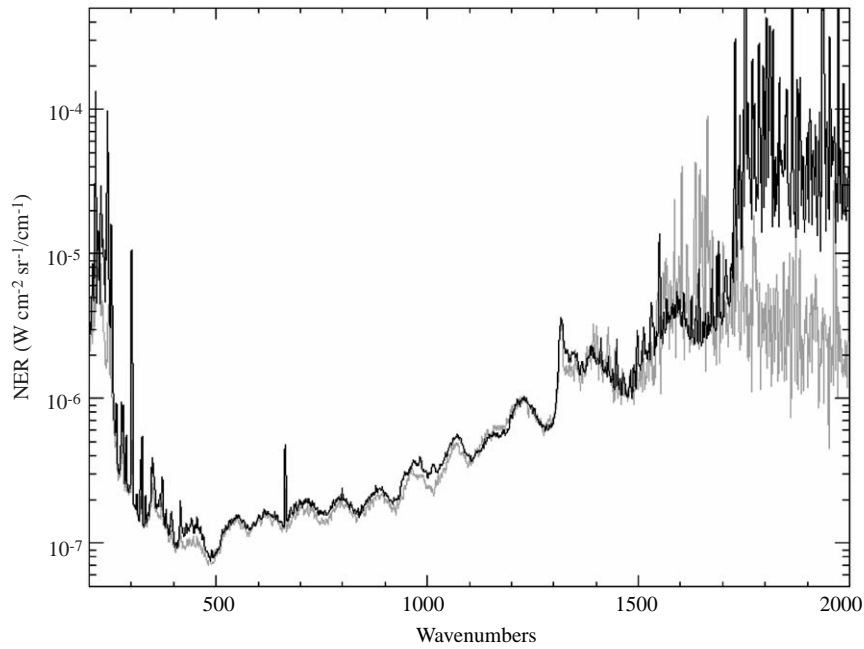


Fig. 7. NER obtained from IFSI (black curve—sources warmer than the detector temperature) and IKI (grey curve—sources colder than the detector temperature) blackbody measurements.

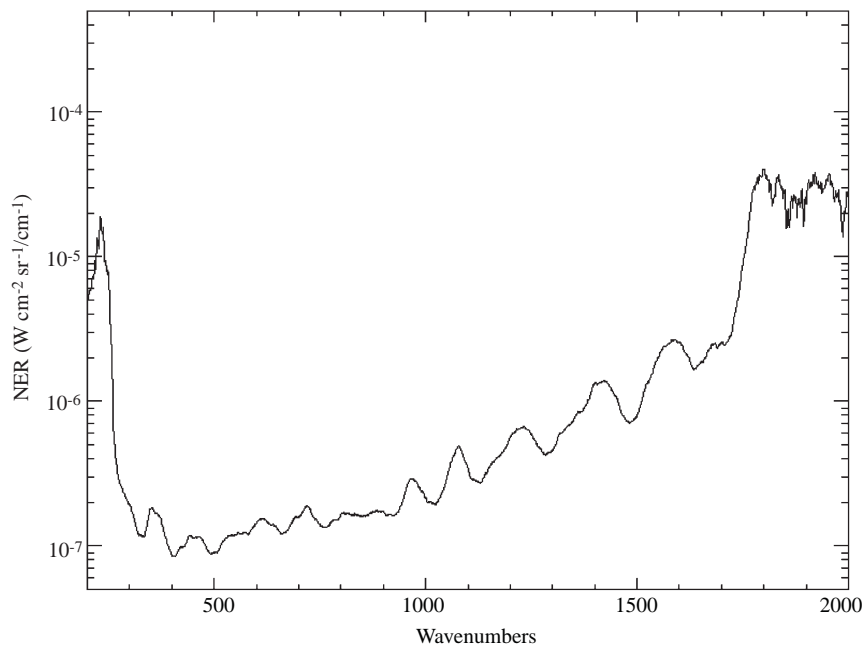


Fig. 8. NER obtained from the internal blackbody measurements in the thermovacuum chamber.

maximum imposable value (see Fig. 3), in space, the LW detector temperature is fixed and stable between 286.9 and 287.0 K, i.e. 286.95 ± 0.005 K, allowing measurements in controlled conditions. The typical interferometer temperature behaviour during the NEV phase is shown in Fig. 4: after more than three and a half hours (an acquisition every 10 s) it increases by about 4 K, varying from 281 to 285 K.

To get the spectral responsivity of the instrument, the same approach as used on Earth and described in Section 3.1 was found to provide optimal results and an excellent description of the detector–instrument–source interaction: using the internal blackbody and deep-space measurements, acquired during the whole NEV activity, we obtain practically identical responsivity curves when α is 0.03, that means that the emission of the instrument

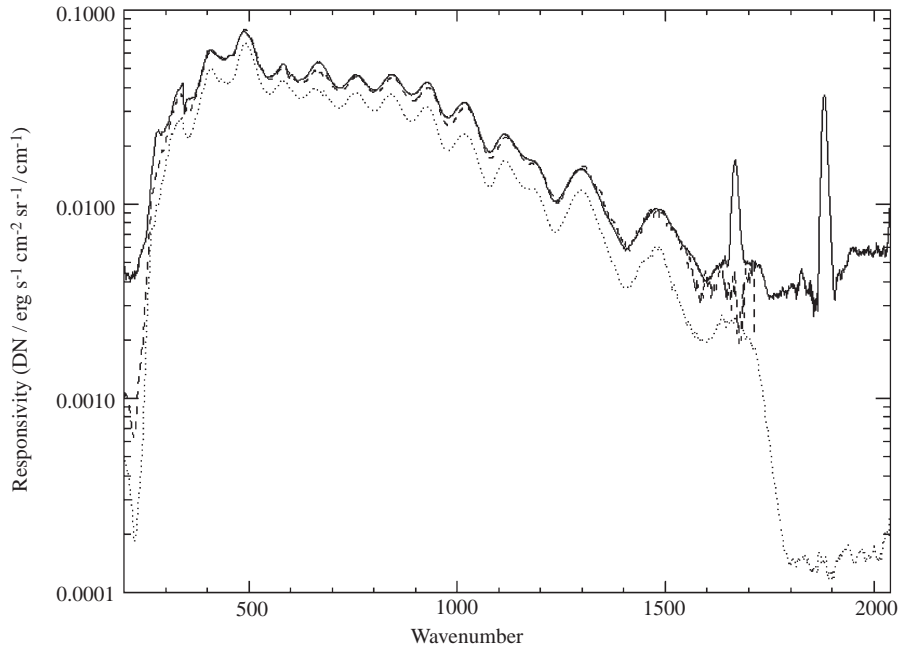


Fig. 9. Comparison between space responsivity (line), laboratory responsivity with IFSI blackbody (dotted) and IKI blackbody (dashed). This last curve has been truncated at 1700 cm^{-1} for picture clarity.

$I_o(\nu)$ is controlled primarily by the detector temperature. Eq. (3.3) then becomes

$$R(\nu) = \frac{S(\nu)}{I(\nu) - 0.03 \cdot B(T_i, \nu) - 0.97 \cdot B(T_d, \nu)}. \quad (3.6)$$

In Fig. 9 we show the NEV results, together with the responsivities previously calculated in the laboratory with the IKI and the IFSI blackbodies for comparison (the same as in Fig. 5). The NEV responsivity is between 0.005 and $0.08\text{ DN/ergs}^{-1}\text{ cm}^{-2}\text{ sr}^{-1}/\text{cm}^{-1}$ over the whole wave number range $200\text{--}2000\text{ cm}^{-1}$. The agreement with the IKI blackbody responsivity is almost perfect (as it should be since both deep-space and the internal blackbody are colder than the detector, and so was the IKI blackbody), with some differences in the $200\text{--}400\text{ cm}^{-1}$ range and above 1600 cm^{-1} , where the IKI BB responsivity is not well defined (see also Fig. 5). The NEV responsivity also has two large peaks in correspondence of the frequencies of mechanical vibrations generated by the spacecraft reaction wheels. These disturbances are not directly introduced in the frequency range in which we are operating ($75\text{--}750\text{ Hz}$ with pendulum speed at 2500 Hz , see Paper 1), but are introduced through aliasing.

The constancy of the responsivity between prelaunch tests and NEV activity is a good indication that optical alignment has not suffered during the launch phase and the transit period to Mars, and that, thanks to the gas-tight box, the CsI beamsplitter has maintained its optical properties.

The responsivity obtained by means of Eq. (3.6) has been used to calibrate measurements of the internal blackbody. Fifty measurements have been averaged and compared with the Planck function for the same temperature ($\sim 265.4\text{ K}$) and then smoothed over 11 points for a better comparison (Fig. 10); it appears that the instrument is able to measure radiance in the entire range $200\text{--}2000\text{ cm}^{-1}$. The mechanical vibrations disturb the measurements by increasing the noise in the range of frequencies affected by them.

In space the detector temperature and the interferometer temperature are substantially different; this allows us to describe the detector–instrument–source interaction in a more consistent way so that we take into account such temperature differences. We can consider both the detector and the instrument as blackbodies, each with its effective emissivity. The instrument emits toward space and the detector, which is, in turn, also emitting toward space. Eq. (3.1) can be then rewritten as follows:

$$|S(\nu)| = R(\nu)|I(\nu) + \varepsilon_i(\nu)B(T_i, \nu) - \varepsilon_d(\nu)B(T_d, \nu)|. \quad (3.7)$$

With this approach, we will need four measurements to be able to calibrate the Martian radiation (one of the four). When at Mars, we are going to have a complete set of calibration spectra at the beginning of each session, and another one at the end of the session. A priori these two sets could be equal, but we know by experience that, while the detector temperature will be constant over the 2 h (this will be the duration of each session), the instrument temperature will not (see Fig. 4);

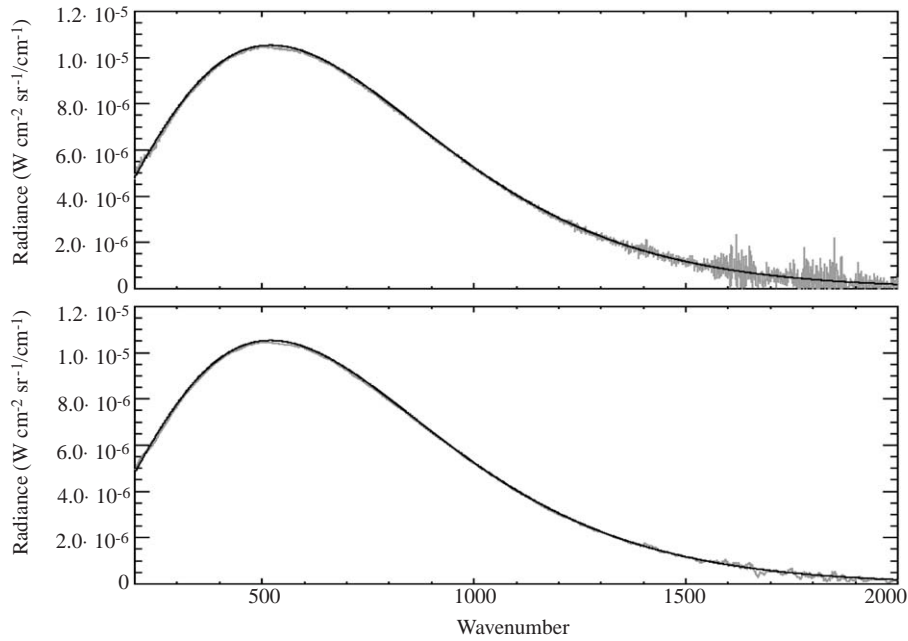


Fig. 10. Top: 50 measurements averaged radiance of the internal BB. Bottom: same curve smoothed over 11 points. Black curves are theoretical Planck functions. Note the perfect matching over the entire range.

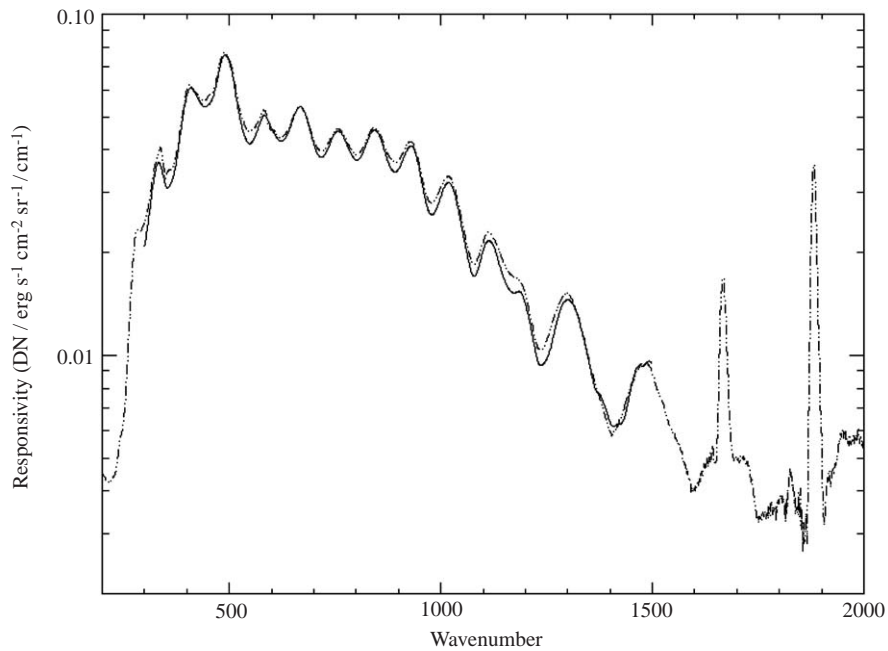


Fig. 11. Comparison between the responsivities obtained with Eqs. (3.6) (dash dot-dot) and (3.7) (line). This last curve is limited in the 300–1500 cm^{-1} spectral range, which is less affected by noise.

therefore we can, at every pass, get the needed four measurements. During the fifth day of NEV tests we obtained two deep-space and two internal blackbody observations with some temperature differences between the two pairs. We have computed first the four average spectra and then, by means of Eq. (3.7), the PFS

responsivity and the radiance of the internal blackbody. Fig. 11 shows the comparison between the responsivities obtained with Eqs. (3.6) and (3.7); the curves are very similar although the one obtained with this last approach is more noisy outside the 300–1500 cm^{-1} spectral range. Some differences can be seen in the

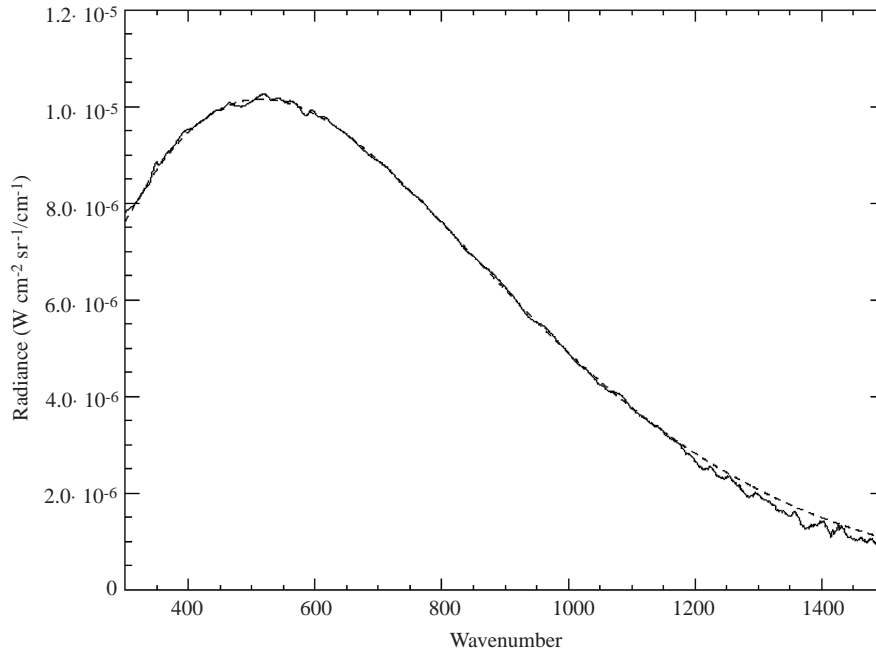


Fig. 12. Radiance of the internal blackbody obtained using Eq. (3.7) (line) compared with a theoretical Planck function of the same temperature (dashed).

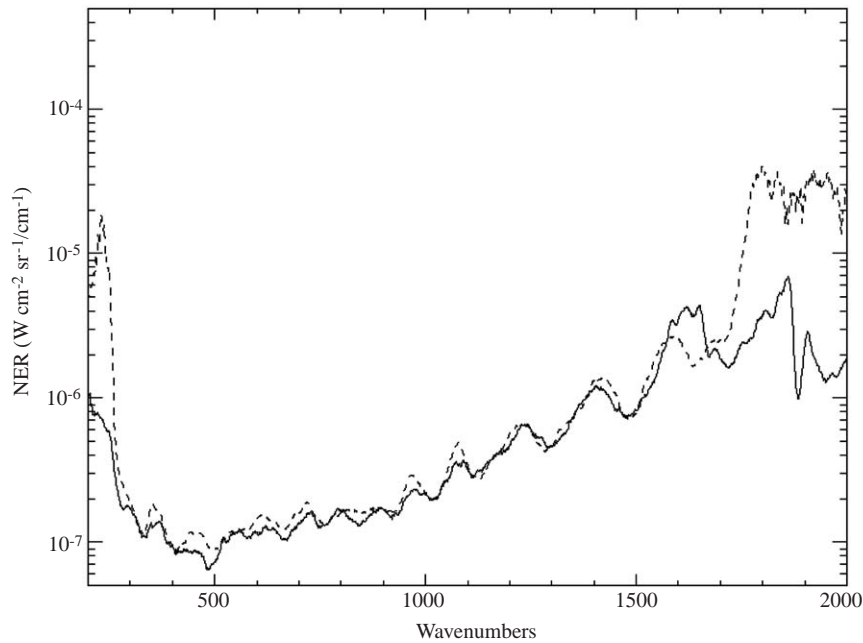


Fig. 13. Comparison between NER computed in space (line) and in laboratory (dashed).

depth of the modulations induced by the spectral characteristics of the optics.

The resulting radiance is compared with a Planck function in Fig. 12; the agreement is good, but spectral features due to optical elements are still visible.

Overall, although the latter is formally more reasonable and physically correct, the same approach as used in laboratory produces better results.

Remarkably enough, the NER in space is practically the same as in the laboratory, a further index of a high stability of the instrument. Moreover, at the borders of the spectral range, namely in the $200\text{--}300\text{ cm}^{-1}$ interval and above 1700 cm^{-1} , where the NEV responsivity is better defined than that obtained in laboratory, the NER is found to be up to 100 times lower (Fig. 13).

3.4. Calibration at speed 2500 Hz

All the studies and results described up to now are referred to the nominal speed 2000 Hz of the double pendulum. As previously said, speed 2500 Hz is going to be the baseline for the future, so we repeated the calibrations at this speed by means of Eq. (3.6).

The different speed implies a different band-pass filter applied to the signals, therefore the spectral shape of the same source is going to be a little different. Naturally, the positions of the peaks induced by the mechanical vibrations will also be different.

Responsivity and NER for the two different speeds are compared in Figs. 14 and 15, respectively.

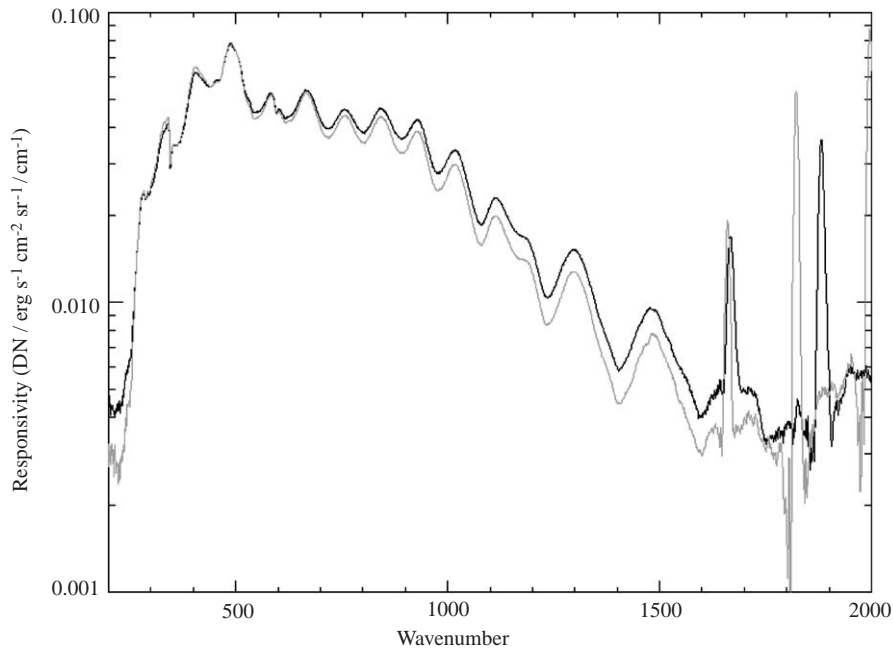


Fig. 14. PFS LWC responsivity at nominal speed (black) and speed 2500 Hz (grey). Eq. (3.6) has been used. Note the difference between the two curves, with the 2500 Hz responsivity being a bit higher before 500 cm⁻¹ and lower above.

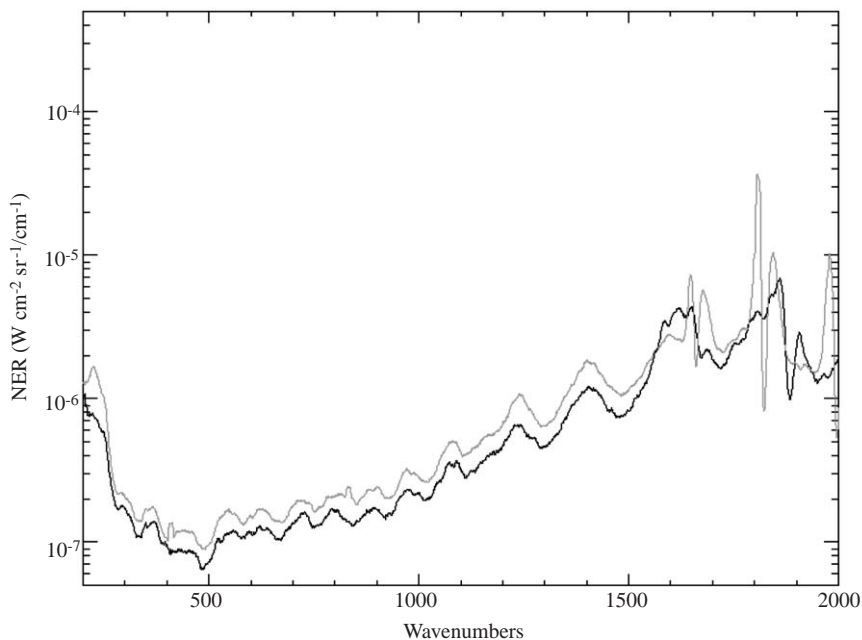


Fig. 15. PFS NER at nominal speed (black) and speed 2500 Hz (grey). The speed has just a little effect on the NER.

3.5. Calibration at Mars

At Mars we have tried to use the previous results, but we always had problems in the sense that the small oscillations due to optical modulations of the signal (having maximum amplitude when looking at deep space, and minimum when Mars had the same temperature of the instrument (287K)) were not eliminated completely, and were introducing spurious features in the calibrated spectra.

We identified then, that Eq. (3.1) can be written as

$$|S(\nu)| = R(\nu)I(\nu) - R^{\circ}I^{\circ}(\nu). \quad (3.8)$$

Essentially, the PFS responsivity looking at deep space should be considered different from the responsivity when looking at Mars. On the other hand, the second term is the measured spectrum looking at deep space. This term is not constant because it depends on the temperature of the interferometer, and this keeps changing during the pericentre pass. Fortunately, we

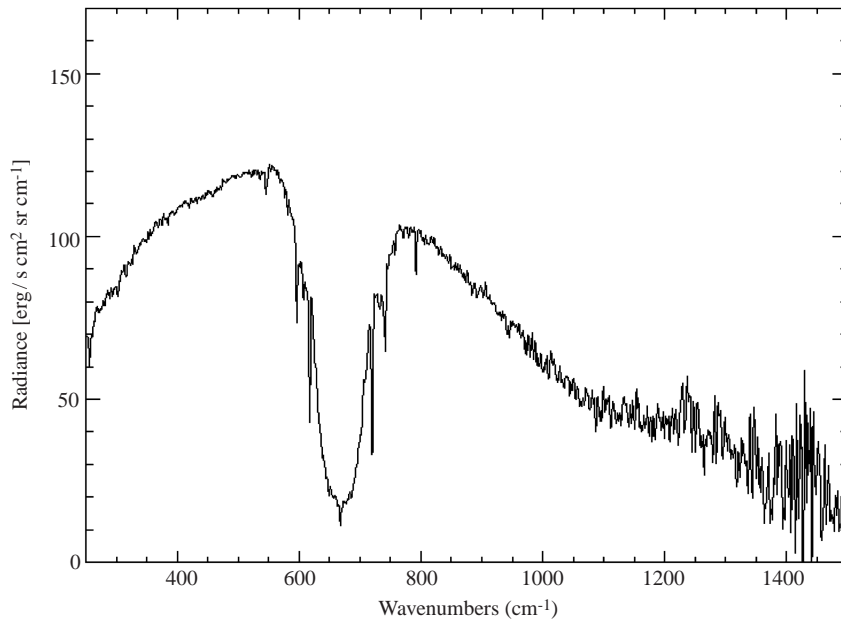


Fig. 16. A single PFS calibrated spectrum of Mars.

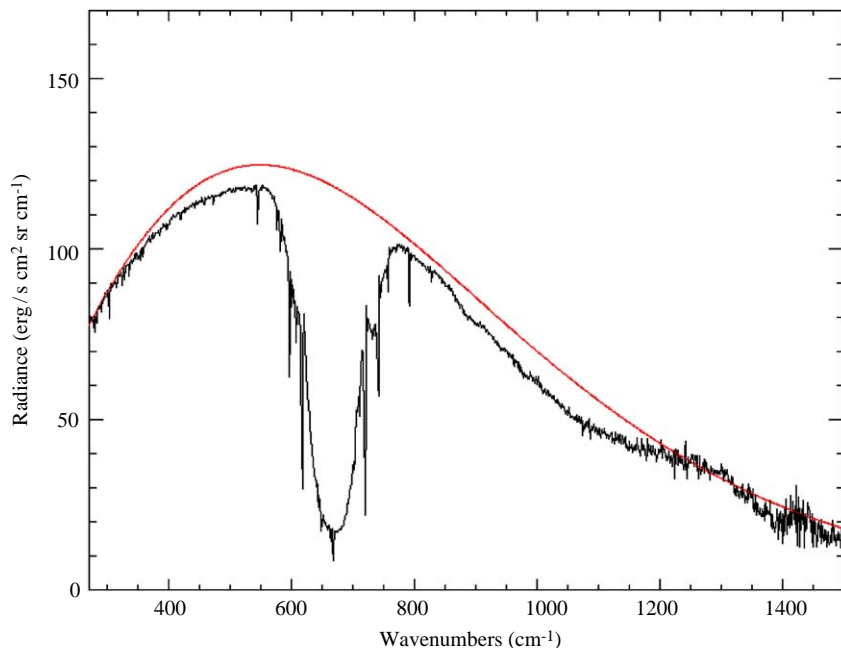


Fig. 17. PFS spectrum (average over 11 measurements) compared with a Planckian.

have Deep Space measurements just before and just after the pass, so we can interpolate the DS spectrum at the temperature measured for each measurement. If we have N measurements, we compute N DS spectra. Eq. (3.8) then provides the Martian radiance if we use the correct responsivity. Sometimes, the Laser Diode temperature also is not constant, therefore we have to resample R (ν previously obtained) at the correct wave

numbers taking into account the temperature (wavelength) of the laser.

We have finally obtained the calibrated thermal radiance emitted by Mars in this way. A typical single spectrum is shown in Fig. 16: the very deep CO_2 $15\ \mu\text{m}$ band is evident, as well as a wide dust band between 850 and $1200\ \text{cm}^{-1}$. In Fig. 17 we show a spectrum (average over 11 measurements) and its Planckian fit.

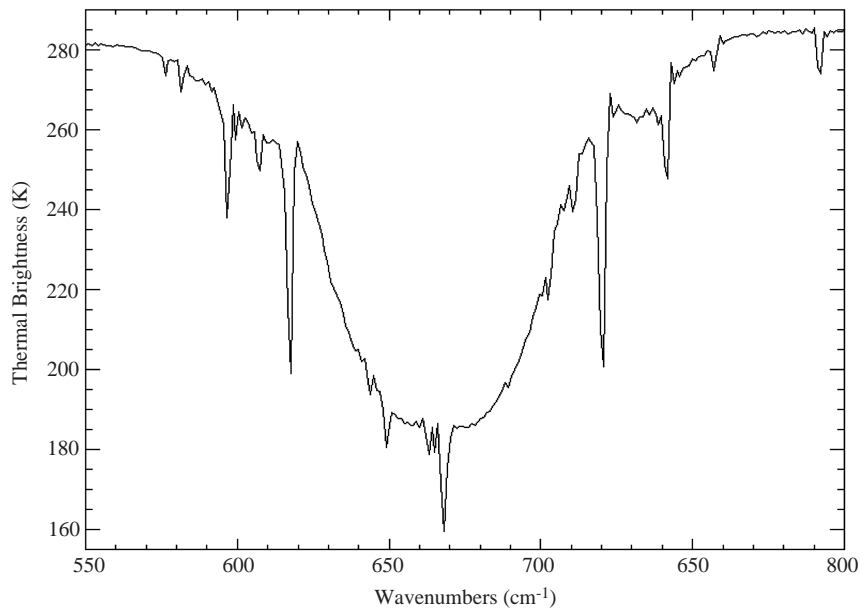


Fig. 18. The same average spectrum of Fig. 17, shown here as a thermal brightness.

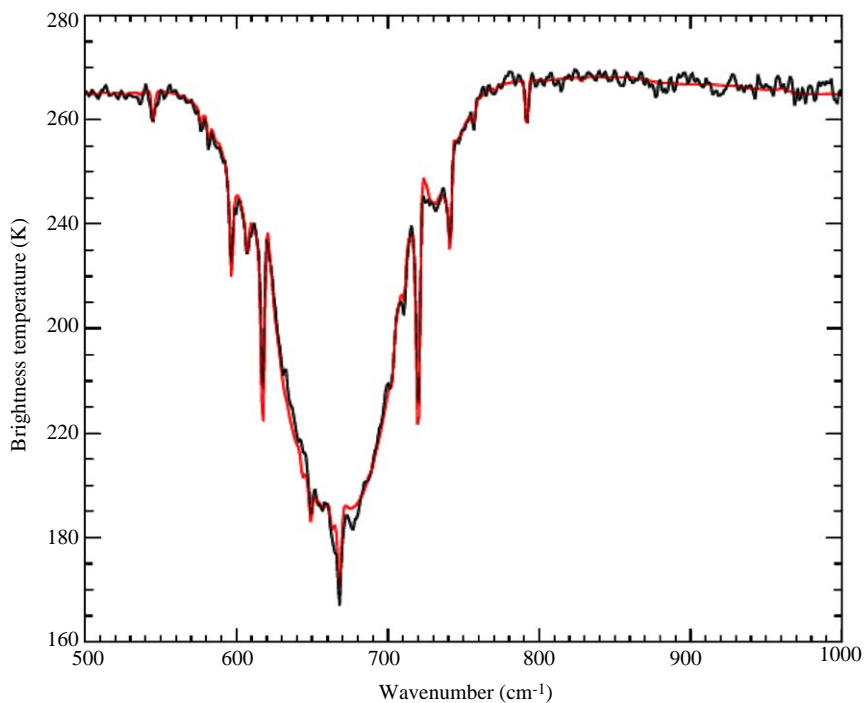


Fig. 19. A single PFS spectrum (black) obtained from apodised (Hamming) interferogram (lower spectral resolution) fitted by a synthetic spectrum (red).

To evidenciate the spectral resolution capability of PFS, we show the bottom of the CO₂ band in Fig. 18. The lines between 660 and 670 cm⁻¹ are the main Q-branch and the isotopic Q-branches. The spectral distance between the isotopic Q-branches in the bottom of the figure is of the order of 2 cm⁻¹, and they are well resolved.

In conclusion, to stress that outside the spectral range affected by the vibration disturbances, all the faint spectral features are reliable, we show in Fig. 19 a single PFS spectrum obtained from an apodised interferogram (Hamming function, lower spectral resolution) fitted by a synthetic spectrum.

References

- Forman, M., Howard, W., 1966. Correction of asymmetric interferograms obtained in the fourier spectroscopy. *J. Opt. Soc. Am.* 56, 59–63.
- Formisano, V., the PFS Team, 2005. The Planetary Fourier Spectrometer (P.F.S.) onboard the European Mars Express Mission, this volume.
- Formisano, V., Mattana, A., Biondi, D., Mencarelli, E., Nespoli, F., Rossi, M., Maturilli, A., Giuranna, M., Grassi, D., Piccioni, G., Saggin, B., Fonti, S., Hirsh, H., 2002. PFS Instrument Calibration Report, vol. I, IFSI internal note.
- Formisano, V., Giuranna, M., Grassi, D., Maturilli, A., Piccioni, G., Saggin, B., Fonti, S., Hirsh, H., Zasova, L., Ignatiev, N., Mattana, A., Biondi, D., Mencarelli, E., Nespoli, F., Rossi, M., 2003a. PFS Instrument Calibration Report, vol. II, IFSI internal note.
- Formisano, V., Mattana, A., Giuranna, M., Biondi, D., Nespoli, F., Mencarelli, E., Rossi, M., Maturilli, A., Piccioni, G., Saggin, B., Michalska, M., Grygorczuk, J., 2003b. PFS Instrument Calibration Report, vol. III—PFS Space Calibration, IFSI internal note.
- Giuranna, M., et al., 2005. Calibration of the PFS SW channel. *Planet. Space Sci.*
- Hanel, R.A., et al., 1992. *Exploration of the Solar System by Infrared Remote Sensing*. Cambridge University Press, Cambridge.
- Hanel, R.A., et al., 1970. Infrared Spectroscopy Experiment for Mariner Mars 1971. *Icarus* 12, 48–62.
- Hanel, R., et al., 1972. Mariner 9 Michelson Interferometer. *Applied Optics* 11 (11), 2625–2634.

Further reading

- Hirsch, H., 1997. Optical design and performance of the Planetary Fourier Spectrometer. *Microchim. Acta* 14 (Suppl.), 571–574.